SCIENTIFIC REPORTS

OPEN

SUBJECT AREAS:
BIOLOGICAL FLUORESCENCE
MEMBRANE BIOPHYSICS
ION CHANNELS IN THE NERVOUS SYSTEM
MOLECULAR MODELLING

Received
21 February 2013

Accepted
28 March 2013

Published
16 April 2013

Correspondence and requests for materials should be addressed to S.W. (shengwang@mail.hust.edu.cn) or J.P.D. (jpding@mail.hust.edu.cn)

* These authors contributed equally to this work.

Inter-α/β subunits coupling mediating pre-inactivation and augmented activation of BK_{Ca}(β2)

Panpan Hou[1]*, Wenping Zeng[1]*, Geliang Gan[1]*, Caixia Lv[1]*, Xiying Guo[1], Zheng Zhang[1], Haowen Liu[1], Ying Wu[1], Jing Yao[1], Aguan D. Wei[2,3], Sheng Wang[1] & Jiuping Ding[1]

[1]Key Laboratory of Molecular Biophysics of the Ministry of Education, College of Life Science and Technology, Huazhong University of Science and Technology, Wuhan, Hubei, 430074, China, [2]Center for Integrative Brain Research, Seattle Children's Research Institute, M/S C9S-10, 1900 Ninth Avenue, Seattle, WA 98101, USA, [3]Department of Neurological Surgery, University of Washington School of Medicine, Seattle, WA 98101, USA.

Large-conductance calcium-activated potassium (BK) channels regulate the electric properties and neurotransmitter release in excitable cells. Its auxiliary β2 subunits not only enhance gating, but also confer inactivation via a short-lived preinactivated state. However, the mechanism of enhancement and preinactivation of BK channels by β2 remains elusive. Using our newly developed methods, we demonstrated that electrostatic forces played a crucial role in forming multiple complementary pairs of binding sites between α and β subunits including a "PI site" required for channel preinactivation, an "E site" enhancing calcium sensitivity and an "E_{CaB}" coupling site transferring force to gate from the Ca^{2+}-bowl via the β2(K33, R34, K35), E site and S6-C linker, independent of another Ca^{2+} binding site mSlo1(D362,D367). A comprehensive structural model of the BK(β2) complex was reconstructed based on these functional studies, which paves the way for a clearer understanding of the structural mechanisms of activation and preinactivation of other BK(β) complexes.

Large-conductance Ca^{2+}- and voltage-activated potassium (MaxiK or BK) channels are ubiquitously expressed in most tissues[1]. As a voltage and calcium sensor[2], BK channels play a critical role in modulating many physiological activities, including neurotransmitter release and endocrine secretion in neurons or endocrine cells, contraction in smooth muscle cells and frequency tuning in hair cells[3–7].

BK channels are tetramers, composed of four Slo1α subunits. Each α subunit has seven transmembrane segments S0-S6 with an extracellular N-terminus and a large cytoplasmic C-terminus that contains a mechanical linker following the S6 pore region[8] and two Rossmann-fold RCK (Regulator of Conductance of K^+) domains with the two sites (calcium bowl and BK(D362,D367)) required for activation by calcium[2,9–11]. Recently, crystal structures of the two RCK domains in both the open and closed states were revealed in two studies[12,13], which further advanced exploration of the gating mechanism of the BK channel by Ca^{2+}.

Native BK-type channels exhibit numerous modified properties after associating with tissue-specific auxiliary β1−β4 subunits. One BK channel can associate with up to four auxiliary β subunits in 1 : 1 stoichiometry with mSlo1α subunits[14,15]. Among the β1–β4 subunits, the β2 and β3b subunits not only modulate activation of BK channels, but also inactivate its currents[16–18]. Moreover, both β2 and β3b subunits result in a distinct outward rectification of BK currents owing to several basic residues located at the middle of the extracellular loops[19,20]. The inactivation domain (ID) of the β2 NH2-terminus, composed of a hydrophobic head group Phe-Ile-Trp (FIW), interacts with a superficial site near the cytoplasmic mouth of BK channels, leading to N-type inactivation[21]. Additionally, evidence indicates that N-type inactivation induced by either Kvβ1 subunits of Kv1.2, or BK β2 or β3b subunits is generated by a two-step inactivation process[22–24]. This process can be described by a simple kinetic model: C←→O←→O*←→I. Here C, O, O* and I represent the closed, open, short-lived conducting (or preinactivated) and inactivated states, respectively. Even though strong functional evidence for existence of the O* state in mSlo1/β2 channels has been described[22], the preinactivation binding sites of Slo1α and β2 are unknown. In addition, the β2 subunit has recently been identified to interact with the Slo1α N-terminal segment including the S0 segment, and the AC region (βA-αC) of RCK1 domain[25]. However, the detailed mechanism of interaction between Slo1α and β2 subunits remains unclear.

To fully understand the mechanisms of α/β interactions, four approaches were jointly used to identify multiple complementary pairs of a preinactivation PI site and an enhancing calcium sensitivity E site with a signal transduction pathway via an E_{CaB} site coupling to the calcium-bowl in the cytosolic region of α and β subunits, which provides a comprehensive model of how the mSlo1α subunit functions in concert with the β2 subunit. Our methods may be usefully extended to reveal and confirm interaction sites between subunits in other multimeric membrane protein complexes.

Results

Modulation of BK-type channel gating by β2 subunits involves both membrane-spanning and cytoplasmic domains of mSlo1[25]. To better understand the dynamic structural interactions within the BK(β2) complex during gating, we focused on putative cytosolic binding sites formed by the β2 N-terminal segment and the mSlo1α subunit.

Specific β2 mutations change the structural configuration of β2-mSlo1 complex. In previous studies, we scanned the entire N-terminal of the β2 subunit and created three interesting β2 mutants, β2(D16R,E17K), β2(E44K,D45R) and β2(D16R,E17K, E44K,D45R) (Figure 1)[18]. Wild-type (WT) BK(β2) channels co-assembled by mSlo1α and auxiliary β2 subunits show rapid inactivation with a significant left-shift of the G–V curve, compared with BK(mSlo1α) channels (Figure 2A–C). When similarly coexpressed with mSlo1α, β2(D16R,E17K) significantly slowed the inactivation time constant (τ_i = 43.0 ms at 100 mV) with little change in G–V curve compared with WT β2 (τ_i = 16.8 ms). By contrast, β2(E44K,D45R) markedly shifted the G–V of activation (+60.3 mV) with kinetics of inactivation (τ_i = 26.3 ms) similar to WT β2. The third mutant β2(D16R,E17K,E44K,D45R) not only shifted the G–V back to that of mSlo1, but also virtually eliminated inactivation (Figure 2A–C). For evaluating changes in G–V curves more accurately, the ID was deleted from the WT β2 and its mutational variants. Thus, two constructs were built for WT β2 and each mutation variant here. One with ID (β2(D16R,E17K)) was used for comparing the inactivation time constant and the other without ID (Δ3-β2(D16R,E17K)) for comparing the G–V curves. To exclude the possibility that changes in both the G–V and τ_i resulted from an altered stoichiometry of β2 per channel due to insufficient expression of β subunit, we carried out experiments varying the expression ratio of β2 and mSlo1α subunits. Results in Figure S1A indicated that the G–V curves of BK(Δ3–β2) did not obviously shift until the co-transfected ratio of Δ3-β2:mSlo1 decreased to 0.1 : 1 from the 2 : 1 ratio used in this study, suggesting that the amount of β2 co-expressed with mSlo1 was about 20-fold more sufficient than necessary to maintain a saturating stoichiometry of β2 per channel for all experiments, consistent with the results reported by Wang et al[15]. These results with the mutant β2(E44K,D45R) are consistent with a decreased binding affinity to mSlo1α subunits compared with WT β2.

Furthermore, we recorded the instantaneous tail currents of WT and mutant β2 to measure the rectification ratio R (Figure 2D-left and Figure S1B), which fully depends upon the number of positively charged lysine in the outer loop of β2 subunits[19]. A summary of the R values revealed that the R of mSlo1/Δ3-β2(D16R,E17K,E44K,D45R) formed by coexpression of mSlo1 and Δ3-β2(D16R,E17K, E44K,D45R) was similar to that of mSlo1 alone (Figure 2D-right), suggesting that the structural configuration of α/β complex is markedly changed.

Preinactivation site of the BK(β2) complex. In Figure 2B, we noticed that the inactivation time constant of mSlo1/β2(D16R,E17K) was slowed substantially to 42.5 ms from 16.8 ms (mSlo1/β2) without shifting the G–V curves, suggesting that β2(D16,E17) may act as a preinactivation site to shorten the inactivation time constant. Previous studies reported that a preinactivated state (O*) exists in Kv1.2(Kvβ) and BK(β2) channels[22–24,26]. The acidic residues at the N-terminal of β2 subunits first bind to basic residues located at the cytosolic surface just outside the pore, producing a preinactivated state, followed by insertion of a hydrophobic N-terminal domain into the ionic conduction pathway to block the pore[22,24,27].

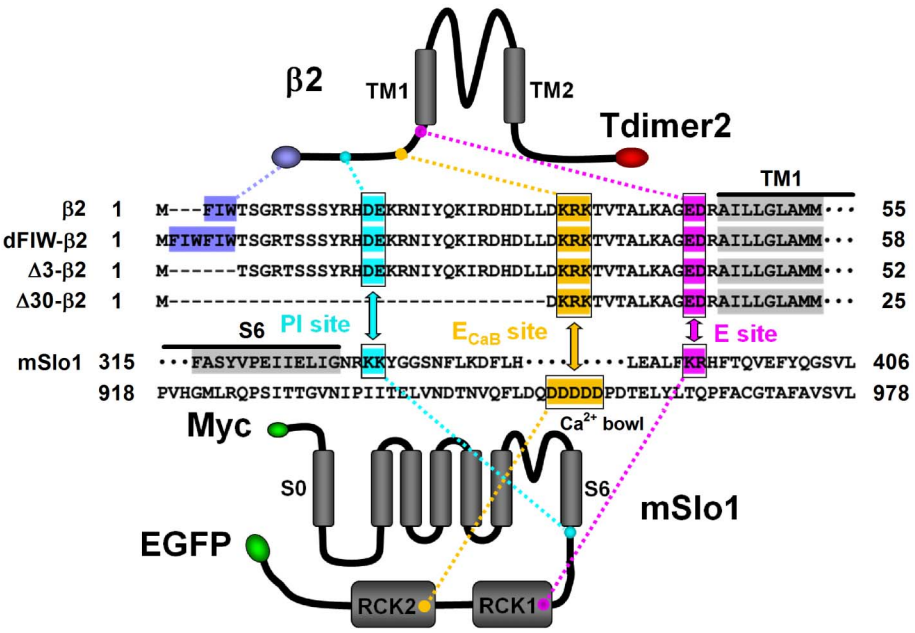

Figure 1 | A Schematic of Different Mutations of mSlo1 and β2 Subunits. Topological maps for mutations of mSlo1α (bottom) and β2 subunits (top) are displayed. The inactivation domain (ID), FIW and FIWFIW (dFIW) are highlighted in slateblue. Tdimer2 (red) and EGFP (green) were attached to the C-terminus of β2 and mSlo1α subunits, respectively, and Myc (green) was inserted at the N-terminus of the mSlo1α subunit. The central panel shows a multi-sequence alignment of β2, dFIW-β2, Δ3-β2, Δ30-β2 and the partial sequence of mSlo1. The boxed amino acids (cyan, orange and pink) in mSlo1 and in the N-terminal of β2, dFIW-β2, Δ3-β2 and Δ30-β2 indicate regions of α/β interaction, termed the preinactivation (PI), electrostatic coupling (E_{CaB}) and enhancing (E) sites as indicated.

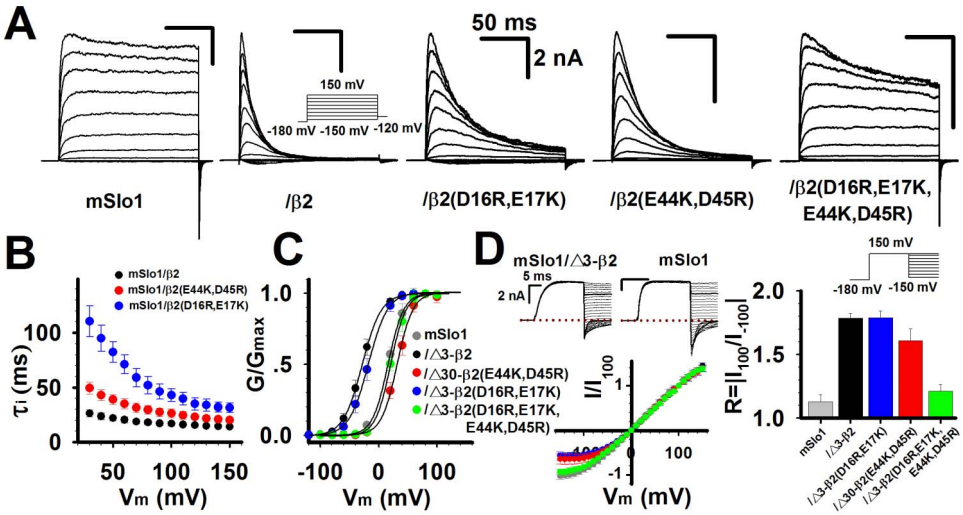

Figure 2 | Differential Modulation by Wild-type and Mutant β2 on mSlo1 Channels. (A) Macroscopic currents of mSlo1 alone and co-expressed with β2, β2(D16R,E17K), β2(E44K,D45R) or β2(D16R,E17K,E44K,D45R) from inside-out patches in the presence of 10 μM Ca^{2+} by the protocol as indicated. (B) Time constants of inactivation (τ_i) of mSlo1/β2 (black), mSlo1/β2(E44K,D45R) (red) and mSlo1/β2(D16R,E17K) (blue) are plotted against membrane potentials. (C) G–V curves for mSlo1 (gray), mSlo1/Δ3-β2 (black), mSlo1/Δ3-β2(D16R,E17K) (blue), mSlo1/Δ30-β2(E44K,D45R) (red) and mSlo1/Δ3-β2(D16R,E17K,E44K,D45R) (green), with 10 μM Ca^{2+}. The V_{50}'s are 18.9 ± 4.6 mV (n = 8), −28.3 ± 5.2 mV (n = 8), −17.7 ± 7.3 mV (n = 8), 32.0 ± 5.3 mV (n = 7) and 20.3 ± 3.7 mV (n = 6), respectively. Solid lines are single Boltzmann functions fitted to each G–V curve. (D) Rectification characteristics of mSlo1 alone (gray) and co-expression with Δ3-β2 (black), Δ3-β2(D16R,E17K) (blue), Δ30-β2(E44K,D45R) (red) and Δ3-β2(D16R,E17K,E44K,D45R) (green). Top left, deactivation currents of mSlo1 and mSlo1/Δ3-β2 activated by protocol as indicated. Bottom left, normalized instantaneous tail currents $I/I_{100\ mV}$ are plotted as a function of activating voltages. Thick black lines among traces represent currents recorded at +100 or −100 mV, respectively. Bottom right, summary of rectification ratios (R), defined as $R = |I_{100\ mV}/I_{-100\ mV}|$, for each individual construct,. The values of R are 1.13 ± 0.06 (n = 10) for mSlo1 alone(gray), 1.78 ± 0.04 (n = 8) for mSlo1/Δ3-β2 (black), 1.80 ± 0.05 (n = 7) for mSlo1/Δ3-β2(D16R,E17K) (blue), 1.61 ± 0.1 (n = 14) for mSlo1/Δ30-β2 (E44K,D45R) (red) and 1.21 ± 0.06 (n = 10) for mSlo1/Δ3-β2(D16R,E17K,E44K,D45R) (green).

To identify the interaction site on mSlo1α corresponding to β2(D16,E17), thermodynamic double-mutant cycle analysis[28–31] was adopted here. Changes of pairwise coupling in free energy between mutations in pairs of residues located in different subunits were respectively calculated by using a thermodynamic square comprised of the WT complex (αβ), the two single mutants (α*β and αβ*) and the corresponding double mutant (α*β*). Here * denotes a mutation. The thermodynamic square was described as follows, $\Delta\Delta G = \Delta G_{\alpha\beta^*} + \Delta G_{\alpha^*\beta} - \Delta G_{\alpha^*\beta^*}$. In such a cycle, if the total free energy change ΔΔG showed a significant change (≥1 kcal/mol), the pairwise residues on α and β subunits would be judged to be coupled[31]. Considering that the free energy of a channel is in direct proportion to V_{50}, we can measure the corresponding V_{50} instead. Thus, this method can be described by the following equation: $\Delta\Delta V_{50} = \Delta V_{50-\alpha\beta^*} + \Delta V_{50-\alpha^*\beta} - \Delta V_{50-\alpha^*\beta^*} - \Delta V_{50-\alpha\beta}$. A distinct change of $\Delta\Delta V_{50} \geq 20$ mV (or 1 kcal/mol) would be judged to be coupled, otherwise, not.

The first candidate of preinactivation sites was mSlo1(K330,K331) because it is the closest cluster of basic residues near the entrance of the cytosolic mouth. Their G–V curves with the corresponding currents of mSlo1(K330,K331) vs β2(D16,E17) cycle are shown in Figure 3A–B, yielding a $\Delta\Delta V_{50} \geq +40$ mV at 10 μM Ca^{2+}, which indicated an obvious interaction. Considering the Ca^{2+} sensitivity of BK channel gating, we repeated the experiments in 1 and 100 μM Ca^{2+} (Figure 3C). The statistics indicate that the $\Delta\Delta V_{50}$ or coupling between mSlo1(K330,K331) and Δ30–β2(D16,E17) is independent of Ca^{2+} (Figure 3C). Moreover, we applied this method to Q- or A-mutations of neighboring residues surrounding β2(D16,E17): mSlo1(R342,K343), mSlo1(K361), mSlo1(K366) and mSlo1(R368) (Figure 3D). None of these assayable mutations showed a $\Delta\Delta V_{50} \geq 10$ mV, with the exceptions of mSlo1(K366A) which failed to express in HEK293 cells. More details about the above results are shown in Figure S2.

A mutation β2(W4E) was previously used to support the existence of preinactivated state (O*) of BK(β2) based on the fact that it has an enhanced probability of very brief openings at steady-state[22]. However, the structural basis of O* was not further identified. To better understand the preinactivation process, we recorded macropatches from the mutation β2(W4E,D16R,E17K), which showed slower inactivation with a higher steady-state offset currents relative to β2(W4E) (Figure S3 and Figure 3E–F). To confirm the role of β2(D16,E17) in preinactivation, single-channel recordings were carried out for β2(W4E) (Figure 3E) and β2(W4E,D16R,E17K) (Figure 3F). In Figure 3E, β2(W4E) produced single channels that exhibited a high frequency of brief openings, indicative of a two-step inactivation scheme. In Figure 3F, however, the brief openings were reduced to minimum with β2(W4E,D16R,E17K), consistent with removal of the preinactivation site. Distributions of open times were well-fitted by the sum of two exponential components (Figure 3G–H). The fast and slow components confer an averaged τ = 0.31 ms for β2(W4E) and τ = 2.0 ms for β2(W4E,D16R,E17K), consistent with what we predicated previously. The two major characteristics of preinactivation are acceleration of inactivation and brief openings caused by rapid transitions between I and O* states due to shorten the inactivation-chain length of β2 via formation of α/β2 contacts at the preinactivation sites (Fig. 3E–F, sFig. 3A–C). Similarly, it also happens in the case of mSlo1(K330E,K331E)/β2(W4E,D16R,E17K) (Fig. 3G–H) in which residues in both α and β2 mediating PI formation are mutated but complementary in polarity. In Fig. 3G, mSlo1(K330E,K331E)/β2(W4E) showed no inactivation and no swift transitions, but with a very flickery opening more similar to the burst-like opening of mSlo1(K330E,K331E) itself at +100 mV (sFig. 3). Considering that binding occurs just before channel inactivated, we name the pairwise residues mSlo1(K330,K331)::β2(D16,E17) as a preinactivated (PI) site. Noticeably, the PI site is a transitory binding site, which is either non-functional or inaccessible when the channel is closed.

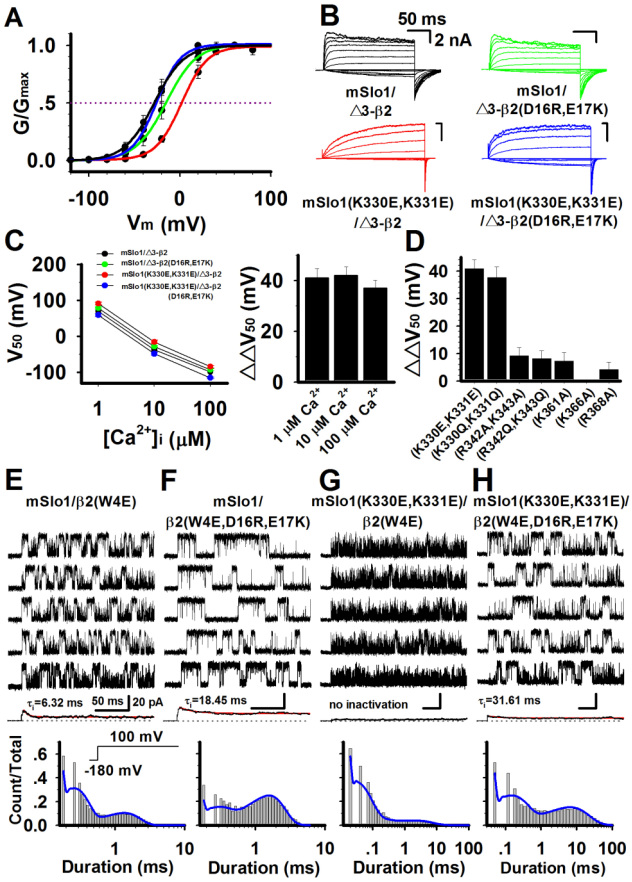

Figure 3 | Transient Preinactivation site mSlo1 (K330,K331)::β2(D16,E17) Determined by Double-Mutant Cycle Analysis. (A) G–V curves are plotted for mSlo1/Δ3–β2 (V_{50} = −28.3 ± 5.1 mV, n = 7, black), mSlo1/Δ3−β2(D16R,E17K) (V_{50} = −16.2 ± 5.2 mV, n = 6, green), mSlo1(K330E,K331E)/Δ3-β2 (V_{50} = 2.9 ± 3.3 mV, n = 7, red), and mSlo1(K330E,K331E)/Δ3-β2(D16R,E17K) (V_{50} = −25.5 ± 6.6, n = 6, blue). Solid lines are single Boltzmann functions fitted to each G–V curve. (B) Representative currents from each experimental combination, recorded from inside-out patches, activated by voltage steps from −160 mV through 220 mV in increment of 20 mV, after a prepulse of −180 mV, in 10 μM Ca^{2+}. (C) The values of V_{50} and $\Delta\Delta V_{50}$ were obtained in 1, 10 and 100 μM Ca^{2+}, respectively. (D) The $\Delta\Delta V_{50}$ are 40.9 ± 3.5 mV(n = 6), 37.6 ± 3.9 mV(n = 6), 9.1 ± 3.1 mV(n = 6), 8.1 ± 2.8 mV(n = 5), 7.2 ± 3.1 mV(n = 5) and 4.1 ± 2.8 mV(n = 6) for Δ3-β2(D16R,E17K) vs mSlo1(K330E,K331E) or mSlo1(K330Q,K331Q) or mSlo1(R342A,K343A), mSlo1(R342Q,K343Q) or mSlo1(K361A) or mSlo1(R368A) in 10 μM Ca^{2+}, respectively. (E–H) Five representative single-channel consecutive traces of mSlo1/β2(W4E), mSlo1/β2(W4E,D16R,E17K), mSlo1(K330E,K331E)/β2(W4E) and mSlo1(K330E,K331E)/β2(W4E, D16R, E17K) recorded from inside-out patches at +100 mV in 10 μM Ca^{2+}. Middle traces show ensemble averages of 100 consecutive sweeps. Initial capacitive currents within the first 0.5 ms of voltage steps were deleted. At the bottom, histogram of open-time durations from the four single-channel recordings were fitted with bi-exponential function with τ_{fast} = 0.048 ms, 87% and, τ_{slow} = 1.83 ms, 13% for mSlo1/β2(W4E), τ_{fast} = 0.061 ms, 36% and τ_{slow} = 2.98 ms, 64% for mSlo1/β2(W4E,D16R,E17K), τ_{fast} = 0.038 ms, 92% and τ_{slow} = 3.32 ms, 8% for mSlo1(K330E,K331E)/β2(W4E) and τ_{fast} = 0.046 ms, 78% and τ_{slow} = 9.86 ms, 22% for mSlo1(K330E,K331E)/β2(W4E,D16R,E17K).

Binding sites between mSlo1 and β2 subunits sorted by immunofluorescence. In previous study, we found that a four-turn α helical segment at the N-terminal of β2, acts as an endoplasmic reticulum (ER)-retention signal, to prevent the surface expression of β2 except when coexpressed with mSlo1α[32]. Interestingly, a mutant dFIW-β2, engineered with an additional N-terminal FIW sequence before β2 (Figure 1), was firmly retained in ER and BK currents were eliminated from the plasma membrane even when coexpressed with either mSlo1-EGFP or Myc-mSlo1 (Figure 4A), suggesting that dFIW is an enhanced retention signal for mSlo1/β2 complexes. Based on these results, we hypothesized that immunofluorescence could be useful employed for assaying a physical separation of α and β subunits within the mSlo1/β2 complex, after deletion or mutation of candidate binding sites required for their co-assembly. For developing this assay, we demonstrated that the fused fluorescent proteins (-EGFP, Myc- and -Tidimer2) did not alter the gating properties of WT channels (Figure S4–S5).

Taking advantage of the enhanced retention signal dFIW, we devised a visual assay for α/β association. We reasoned that mutations in either mSlo1α or β2 subunits which reduced the affinity of α/β association would be directly reflected by the fraction of mSlo1α released from ER-retention to the plasma membrane. The first candidate α/β binding site on β2 tested was composed of residues β2(E44,D45), based upon the observation that β2(E44K,D45R) fully abolished the enhancing Ca^{2+} sensitivity of β2. Where is the corresponding site on mSlo1α which directly interacts with β2(E44,D45)? Several studies suggest that TM1 and TM2 of the β subunit are closely located with Slo1α S2 and S0, respectively[33–35]. Moreover, the crystal structure of the entire cytoplasmic region of BK(hSlo1) has been determined by two distinguished laboratories[12,13]. Therefore, we reasoned that a candidate α/β association site on mSlo1α corresponding to β2(E44,D45) should possess at least some of three features: 1) Positive charges (Arginine (R) or Lysine (K)). 2) Location near the C-terminal end of S2. 3) Location near to or within the RCK1 domain. Based on the above criteria, a series of possible binding sites were tested experimentally (Figure 4). After screening mSlo1α residues (K47), (K59), (K65), (K330,K331), (K392,R393) and (K623,R624), we finally focused on the interaction between mSlo1(K392,R393) and β2(E44,D45), which satisfied the above criteria. After co-transfecting with dFIW-β2(E44K,D45R)-Tdimer2, mSlo1α appeared on the plasma membrane as we predicted (Figure 4B-left). Similarly, co-transfecting Myc-mSlo1 (K392E, R393D) with dFIW-β2-Tdimer2 conferred the same result (Figure 4C-left). The non-inactivated currents recorded from these cells indicated that the affinity of α/β association was significantly decreased by either mSlo1(K392E,R393D) or β2(E44K,D45R) (Figure 4B-C-right). Additionally, we also noticed that dFIW-β2(E44K,D45R)-Tdimer2 was still restricted to the cytoplasm. To further test if α/β association was mediated at this site, we coexpressed Myc-mSlo1(K392E,R393D) with dFIW-β2(E44K,D45R)-Tdimer2, in which the charge polarities in mSlo1α and β2 subunits at the putative α/β association site were reversed but complementary. In this case, we saw small green puncta at the plasma membrane and null currents from recordings (Figure 4D), indicating that most of the mSlo1α complexed with β2 and was retained within the cells. After permeabilizing the cell membrane with Triton X-100, we found that both Myc-mSlo1(K392E,R393D) and dFIW-β2(E44K,D45R)-Tdimer2 were indeed retained and colocalized inside the cell (Figure 4D-left), just as effectively as Myc-mSlo1/dFIW-β2-Tdimer2 (Figure 4A).

With the help of fluorescence imaging, a physical separation of mSlo1α and β2 subunits was achieved by mutations, suggesting that mSlo1(K392,R393) and β2(E44,D45) formed a binding site to enhance the calcium sensitivity of BK(β2) channels. To quantify these results, we collected more data for statistical analysis (Figure 4E). The membrane fluorescence intensity of Myc-mSlo1 for each combination was normalized to the intensity of Myc-mSlo1/β2-Tdimer2, by immunohistochemistry under non-permeabilized condition. By this criteria, fluorescence intensities were: 100%

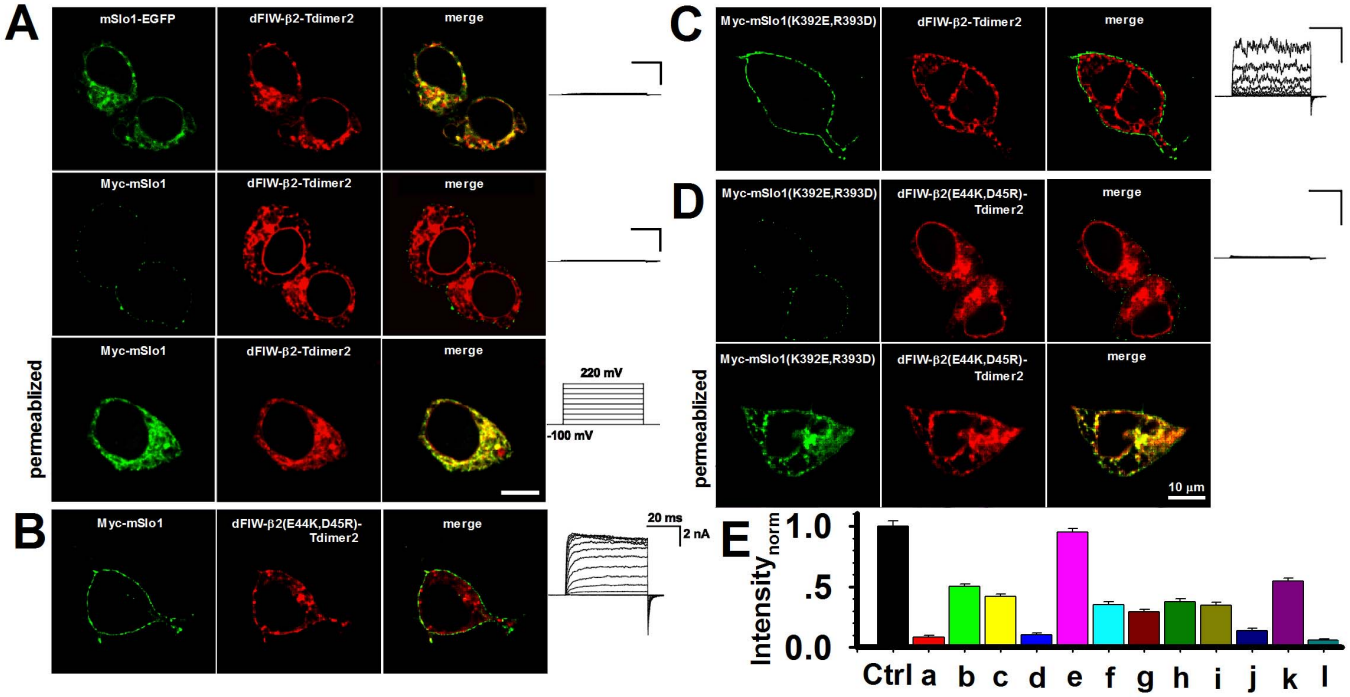

Figure 4 | Immunofluorescence Imaging for an Interacting Set of Complementary mSlo1(K392,R393)/β2(E44,D45). (A–D) Left panels, confocal surface immunofluorescence images of Myc-mSlo1/dFIW-β2-Tdimer2 (A, top), Myc-mSlo1/dFIW-β2(E44K,D45R)-Tdimer2 (B), Myc-mSlo1(K392E,R393D)/dFIW-β2-Tdimer2 (C), and Myc-mSlo1(K392E,R393D)/dFIW-β2(E44K,D45R)-Tdimer2 (D, top) acquired under non-permeabilized condition, A and D bottom showed the total immunofluorescence of each corresponding combination under permeabilized condition. Scale bar represents 10 μm. Right panels, representative currents were obtained in 10 μM Ca^{2+}. Voltage protocol is placed in the middle. (E) Summary of immunofluorescence from Myc-tagged mSlo1 or mSlo1 mutants co-expressed with β2 or β2 mutants. Fluorescence intensity of each combination was normalized to the intensity of Myc-mSlo1/β2-Tdimer2. The error bar is S.E.M. (Also see supplemental information). Ctrl—Myc-mSlo1/β2-Tdimer2 (100 ± 4.3%, n = 205), a—Myc-mSlo1/dFIW-β2-Tdimer2 (8.3 ± 1.3%, n = 312), b—Myc-mSlo1/dFIW-β2(E44K,D45R)-Tdimer2 (50.3 ± 2.1%, n = 282), c—Myc-mSlo1(K392E,R393D)/dFIW-β2-Tdimer2 (39.1 ± 1.8%, n = 181), d—Myc-mSlo1(K392E,R393D)/dFIW-β2(E44K,D45R)-Tdimer2 (10.6 ± 1.3%, n = 181), e—Myc-mSlo1(K392E,R393D)/β2-Tdimer2 (95 ± 3.8%, n = 186), f—Myc-mSlo1(K392E)/dFIW-β2-Tdimer2 (31.5 ± 2.4%, n = 150), g—Myc-mSlo1(R393D)/dFIW-β2-Tdimer2 (28.2 ± 1.9%, n = 177), h—Myc-mSlo1/dFIW-β2(E44K)-Tdimer2 (37.9 ± 2.1%, n = 183), i—Myc-mSlo1/dFIW-β2(D45R)-Tdimer2 (34.7 ± 2.2%, n = 157). j—Myc-mSlo1/dFIW-β2(D16R,E17K)-Tdimer2 (15.8 ± 2.0%, n = 201), k—Myc-mSlo1/dFIW-β2(D16R,E17K,E44K,D45R)-Tdimer2 (56.0 ± 2.6%, 28.3, n = 201), l—Myc-mSlo1(K330E,K331E)/dFIW-β2-Tdimer2 (5.8 ± 1.1%, n = 158).

for Myc-mSlo1/β2-Tdimer2 (control, black), 8.3% for Myc-mSlo1/dFIW-β2-Tdimer2 (a, red), 50.3% for Myc-mSlo1/dFIW-β2(E44K,D45R)-Tdimer2 (b, green), 39.1% for Myc-mSlo1 (K392E,R393D)/dFIW-β2-Tdimer2 (c, yellow), 10.6% for Myc-mSlo1(K392E,R393D)/dFIW-β2(E44K,D45R)-Tdimer2 (d, blue), and 95% for Myc-mSlo1 (K392E,R393D)/β2-Tdimer2 (e, pink). These results indicate that residues mSlo1(K392,R393) and β2(E44,D45) pair formed a binding site mediating mSlo1α and β2 subunit assembly. For Myc-mSlo1/dFIW-β2(D16R,E17K)-Tdimer2(15.8%, j, dark blue), the average fluorescence intensity of the discrete green puncta at the plasma membrane was only a little higher than that of Myc-mSlo1/dFIW-β2-Tdimer2. Therefore, β2(D16,E17) does not appear to participate in a α/β association site. Similar results were also observed with mSlo1(K330,K331) (5.8%, l, dark cyan).

Determination of the binding site mSlo1(K392,R393)::β2(E44, D45) and the enhancing calcium sensitivity pathway. To confirm and quantitate the interaction between these two residues, we similarly introduced double-mutant cycle analysis. All G-V curves of the mSlo1(K392,R393) vs β2(E44,D45) cycle were shown in Figure 5A. The total change of $\Delta\Delta V_{50}$ was about +70 mV, suggesting that a strong coupling exists between the mSlo1 (K392,R393) and β2(E44,D45). A summary of $\Delta\Delta V_{50}$ shows that it is independent of Ca^{2+} again (Figure 5D). Altogether, considering that both mSlo1 (K392E,R393D) and Δ30-β2(E44K,D45R) exhibited a significant change in BK channel activation, and that the mutant Δ30-β2(E44K,D45R) abolished the enhancing effect on calcium sensitivity of β2 at 10 μM Ca^{2+} (Figure 2C). The same results were also obtained at 0-300 μM Ca^{2+} (Figure 6). Therefore, we defined the complementary paired residues mSlo1(K392,R393)::β2(E44,D45) as an enhancing (E) site.

It is interesting to further explore how the E site enhances the calcium sensitivity of BK(β2). Using the mutants mSlo1(5D5N) and mSlo1(D362A,D367A) to remove the calcium binding sites, we examined whether the enhancement by E site was blocked. In Figure S6, a series of activation currents are plotted for the mutants mSlo1(5D5N) and mSlo1(D362A,D367A) combined with the Δ30-β2 and Δ30-β2(E44K,D45R). The V_{50}-$[Ca^{2+}]_i$ curve indicates that the calcium bowl changes the calcium sensitivity of BK when the E site is formed (Figure 6A). On the contrary, the V_{50}-$[Ca^{2+}]_i$ curve indicates that mSlo1(D362,D367) does not alter the calcium sensitivity of BK by a functional E site (Figure 6B). Thus, we inferred that the E site enhanced the calcium sensitivity of BK(β2) only via the Ca^{2+} bowl pathway.

Additional experiments were performed to demonstrate that the Δ30-β2(K33,R34,K35) interacted directly with the Ca^{2+}-bowl based on the $\Delta\Delta V_{50}$ = 58 mV at 10 μM Ca^{2+} (Figure 6C–D). In Figure 6E, β2(K33,R34,K35) is just located immediately above the Ca^{2+}-bowl, within distance to form the E_{CaB} site. Consequently, a model revised from Magelby's lab[8] is used to illustrate the mechanism of enhancing

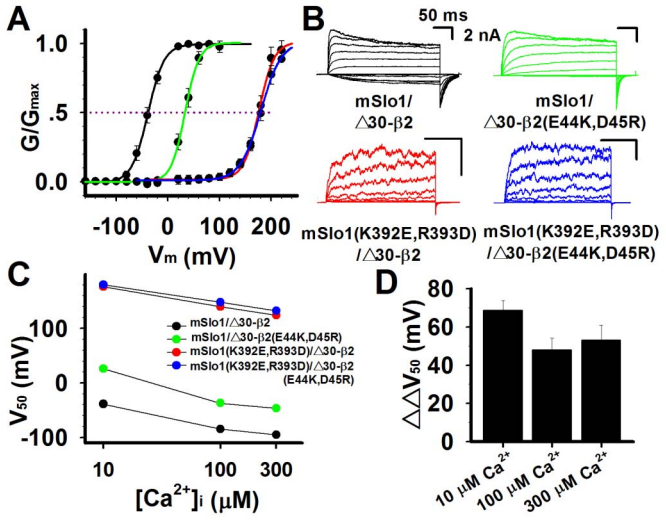

Figure 5 | Interaction between mSlo1(K392,R393) and β2(E44,D45) Determined by Double-Mutant Cycle Analysis. (A) G–V curves plotted for mSlo1/Δ30-β2 (V_{50} = −38.6 ± 5.0 mV, n = 7, black), mSlo1/Δ30-β2(E44K,D45R) (V_{50} = 33.3 ± 6.6 mV, n = 6, green), mSlo1(K392E,R393D)/Δ30-β2(V_{50} = 177.0 ± 6.9 mV, n = 7, red), and mSlo1(K392E,R393D)/Δ30-β2(E44K,D45R) (V_{50} = 180.3 ± 5.0 mV, n = 7, blue). Solid lines are single Boltzmann functions fitted to each G–V curve. (B) Macroscopic currents of each combination were recorded from inside-out patches in 10 μM Ca^{2+} as described in Figure 3B. (C) The values of V_{50} were obtained in 10, 100 and 300 μM Ca^{2+}, respectively. (D) The $\Delta\Delta V_{50}$ of mSlo1(K392E,R393D) vs β2(E44K,D45R) are 67.9 ± 5.1mV n = 6; 42.7 ± 6.1mV, n = 6 and 49.3 ± 7.8mV, n = 6 in 10, 100 and 300 μM Ca^{2+} as indicated.

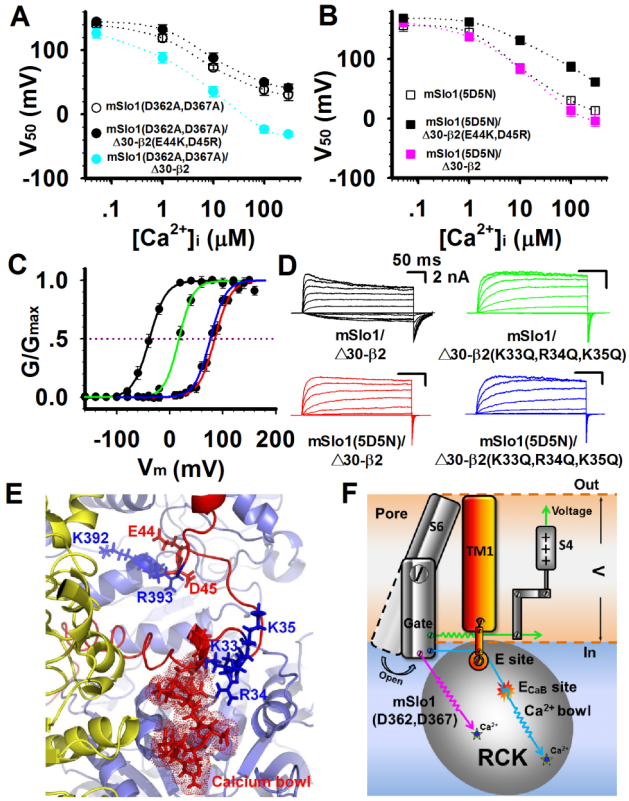

Figure 6 | Signal Transduction Pathway of the Enhanced Calcium Sensitivity in the RCK Domain of BK(β2) Channels. (A) The V_{50} of mSlo1(D362A,D367A) alone (open circle), mSlo1(D362A,D367A)/Δ30-β2 (cyan circle) and mSlo1(D362A,D367A)/Δ30-β2 (E44K,D45R) (filled circle) were measured in 0, 1, 10, 100 and 300 μM Ca^{2+}. (B) The V_{50} of mSlo1(5D5N) alone (open square), mSlo1(5D5N)/Δ30-β2 (pink square) and mSlo1(5D5N)/Δ30-β2(E44K,D45R) (filled square) were measured in 0, 1, 10, 100 and 300 μM Ca^{2+}. (C) The G–V curves are plotted for the mSlo1/Δ30-β2 (V_{50} = −34.6 ± 4.1 mV, n = 8) (black), mSlo1/Δ30-β2(K33Q,R34Q,K35Q) (V_{50} = 17.3 ± 5.6 mV, n = 6) (green), mSlo1(5D5N)/Δ30-β2 (V_{50} = 84.1 ± 4.4 mV, n = 6) (red) and mSlo1(5D5N)/Δ30-β2(K33Q, R34Q,K35Q) (V_{50} = 78.0 ± 6.5 mV, n = 6) (blue). The $\Delta\Delta V_{50}$ is 58.0 ± 8.7 mV at 10 μM Ca^{2+}. (D) The representative traces of the G–V curves shown in (C). (E) An expanded view of the spatial distribution of the calcium bowl, β2(K33,R34,K35), mSlo1(K392,R393) and β2(E44,D45). (F) Hypothetical mechanism showing the pathway of the enhanced calcium sensitivity in BK(β2) Channels. Gray and red parts denote the mSlo1α and β2 subunits, respectively. Colored stars denote two Ca^{2+} binding sites of BK. Green, pink and cyan springs denote the voltage gating, mSlo1(D362,D367) and Ca^{2+} bowl pathways, respectively. The E site serves as a fixed pulley(red circles) in the Ca^{2+} bowl gating pathway via a coupling between E_{CaB} site and Ca^{2+}-bowl, and then optimizes the direction of the gating force, which leads to opening the channel more easily by Ca^{2+}.

calcium sensitivity by β2 (Figure 6F): the Ca^{2+}-bowl exerts a force onto the BK S6 gate, augmented by formation of the E_{CaB} site. By this model, the E site acts in a similar fashion to exert supplemental lateral force onto the gating ring to open the gate via the S6-C linker. This model may help to explain both Ca^{2+}-dependent and Ca^{2+}-independent mechanisms for enhancing gating by β2.

More details about the mechanisms of pre-inactivation and augmented activation of large conductance Ca^{2+}-activated (BK/β2) K^+ channel complexes can be found in the Movie S1.

Discussion

There is a significant diversity in the functional characteristics of BK-type channels mainly due to their association with β subunits which underlies their diverse physiological roles in neural cells. Owing to lack of detailed structural information of the mSlo1α/β complex, their coupling mechanism has been a major long-standing puzzle. In this study, we unequivocally demonstrated that three complementary pairs of residues played critical roles in activation pathway and preinactivation of the mSlo1/β2 complex and developed two novel approaches for further exploring the nature of inter-subunit interactions in ion channels.

Conceivably, this E site, serving as an extra pivot or a scaffold between the membrane-spanning and RCK domains of mSlo1, boosts the channel gating force from the calcium bowl via the C-linker of S6 segment[8], but mSlo1(D362,D367) site delivers the force independently probably due to lack of electrostatic connection as E site does. This also explains why β2 does not potentiate BK channel gating at 0 Ca^{2+}. Considering that the β2(E44,D45) residues are conservative within the BKβ family, it is interesting to investigate different mechanisms of enhancing Ca^{2+} sensitivity of BK channels between β1 and β2[36].

To form the PI site at least four conditions must be satisfied: 1) the PI site of mSlo1 must be near the pore; 2) It must move while the pore opens; 3) It must be positively charged; 4) The PI site on the N-terminal of β must be negatively charged. Based on that, we hypothesize that β3b should have a PI site near the region of β3b (D17 or D19), mimicking that of β2(D16,E17). However, the positive charges of the PI site may accelerate inactivation due to electrostatic effects, if the ID of β subunits is negatively charged. Compared with WT β2 (Figure 2B), for instance, W4E shows faster inactivation (Figure 3E). Therefore, changes in inactivation time constants cannot be an exclusive criterion for conclusively identifying PI sites. Without satisfying the above conditions, inactivation of channels cannot proceed according to the two-step inactivation mechanism.

In this study, we developed a novel approach (Retention-Release) to directly visualize a dissociating process of the mSlo1α/dFIW-β2 complex stably retained in ER, after mutating one of binding sites. Here the retention signal is the hydrophobic FIW-FIW motif in β2, which might anchor to the unknown trafficking or ER-resident proteins to prevent the mSlo1/dFIW-β2 complex from exiting the ER. This approach opens access for the identification of binding sites *in vivo* by a simple visual screen for spatial separation after mutating the binding site. Therefore, this may be a very useful general approach for studying *in vivo* protein-protein interactions, especially for multimeric membrane proteins. This completely differs from the standard co-immunoprecipitation method, which may give artifactual results[10]. The second approach (Rectification) is to utilize the changes on the rectification property of channels to test the binding site. Rectification of BK(β2) comes from the special distribution of basic residues in the loop of β2 subunits[19]. When removing binding sites, it usually disturbs the charge distribution to alter the rectification of channels. Notably, sometimes the rectification changes, but the gating not. In this case, it will be a powerful tool for studying this project.

Methods

Constructs and mutations. For construct of mSlo1-EGFP, EGFP in pEGFP-N1 (Clontech) was cut by two restriction enzymes and subcloned into pcDNA3.1(+) (Invitrogen). Then, mSlo1 was fused in-frame to the N-terminus of the EGFP using appropriate restriction enzymes. Using the same method, a series of constructs in hβ2 were obtained. β2-Tdimer2 was ligated into the pcDNA3.1 vector. Tdimer2 is a red fluorescence protein derived from DsRed[37]. For dFIW-β2-Tdimer2, we added another "FIW" to the N-terminus of β2-Tdimer2 and subcloned into pcDNA3.1 using PCR-based techniques. The Myc-mSlo1 construct was created by adding the sequence of Myc (EQKLISEEDL) in the forward primer and then subcloned into pcDNA3.1. Truncations of the β2 subunit, Δ3-β2 and Δ30-β2, were generated by removing amino acids from positions 2 through 4 and from positions 2 through 31,respectively. Mutations were introduced using QuickChange Site-Directed Mutagenesis Kit (Stratagene). All constructs and point mutations were verified by direct DNA sequence analysis. Figure 1 shows the topological map of the constructs and mutations for all the experiments.

Immunofluorescence and confocal microscopy. About 20 hours after transfection, cells were fixed with 2% paraformaldehyde in PBS for 10 min. For cell permeabilization, 0.1% Triton X-100 was added for 10 minutes. After blocking with 5% FBS for 1 hour, cells were incubated with mouse monoclonal anti-human Myc antibody (1:300) (Abcam) overnight at 4°C. Then cells were washed (2.5% FBS in PBS, 5 min ×6), and incubated with FITC-conjugated goat anti-mouse IgG (H + L) (1:300) (Proteintech) for 2 hours at RT. Non-specific secondary antibodies were removed by washing with PBS (5 min, ×6), followed by a final soak in PBS. Cells were visualized by confocal laser scanning microscopy (Olympus IX71) using a 100× oil immersion lens (NA1.30). Parameter selection, sample scanning and image acquisition were all controlled by Andor IQ 2 software.

Image analysis and statistics. In experiments with coexpressed Myc-mSlo1 (green) and β2-Tdimer2 (red), four cases were seen: No fluorescence, green fringe, red cytoplasm, and red cytoplasm with green fringe. For statistical analysis, we ignored cells with no fluorescence or with only green fringe, due to no expression or expression of only Myc-mSlo1 in HEK293 cells. Fluorescence intensity of the green fringe was calculated by Image J software under non-permeabilized condition, and normalized to the intensity of Myc-mSlo1/β2-Tdimer2. Representative images in figures were dealt with AutoQuantX2. The error bar is S.E.M.

Patch clamp recording. For recordings, transfected HEK293 cells were transferred one day after transfection to 160 K^+ solution containing (in mM): 160 $MeSO_3K$, 2 $MgCl_2$, 10 HEPES(PH 7.0). All experiments were carried out with excised patches, in inside-out recording configuration. Patch pipettes were pulled from borosilicate glass capillaries with resistances of 2–3 megohms when filled with pipette solution. Experiments were performed using an EPC-9 patch-clamp amplifier with its software (HEKA, Germany). Currents were typically digitized at 20 kHz and filtered at 8.5 kHz. And for single channel recordings, currents were digitized at 50 kHz and filtered at 15.7 kHz. During recording, different Ca^{2+} concentration solutions were applied onto membrane patches via a perfusion pipette containing eight solution channels. All experiments were performed at room temperature (22–24°C).

Homology modeling. Full models of BK channels were built by Homology Modeling from known partial crystal structure of ion channels. The complexes of mSlo1 and β2 were assembled and then optimized to a local minimal in energy. During the modeling process, the S1-S6 domain was built from MthK (PDB:1LNQ) and KcsA (PDB:1K4C). The closed state model was from the closed RCK by Yunkun Wu[12] (PDB: 3NAF). The open state model was from the open RCK by Peng Yuan[13] (PDB: 3U6N). The S0 helix of BK and the TM1 of β2 was orientated manually according to Guoxia Liu[33]. The missed loops of RCK and the linker of S0-S1 were also rebuilt and refined. The partial structure of β2 was from the NMR structure (PDB:1JO6) and TM1 helix was built manually and refined by Molecular Dynamics[38] (Gromacs). All of structural models were prepared and rendered by PyMol suites (The PyMOL Molecular Graphics System, Version 1.5.0.4 Schrödinger, LLC.).

Data analysis. Macropatch recording data were analyzed with IGOR (Wavemetrics, Lake Oswego, OR), Clampfit (Axon Instruments, Inc.) and Sigmaplot (SPSS, Inc.) software. Unless otherwise stated, data are presented as mean ± S.D. G–V curves for activation were fitted by the single Boltzmann function with the form: $G/G_{max} = (1 + \exp((V - V_{50})/\kappa))^{-1}$, where V_{50} is the voltage at which the conductance (G) is half the maximum conductance (G_{max}) and κ is a factor affecting the steepness of the activations. Tail current values were measured at ~0.25 ms after the onset of voltage steps from the prepulse potential after settling of the capacitance transient, and then normalized to $I_{100\ mV}$. Single-channel recording data were analyzed with QuB (SUNY at Buffalo).

1. McManus, O. B. & Magleby, K. L. Accounting for the Ca(2+)-dependent kinetics of single large-conductance Ca(2+)-activated K+ channels in rat skeletal muscle. *J. Physiol.* **443**, 739–777 (1991).
2. Schreiber, M. & Salkoff, L. A novel calcium-sensing domain in the BK channel. *Biophys. J.* **73**, 1355–1363 (1997).
3. Brayden, J. E. & Nelson, M. T. Regulation of arterial tone by activation of calcium-dependent potassium channels. *Science* **256**, 532–535 (1992).
4. Fuchs, P. A. & Murrow, B. W. Cholinergic inhibition of short (outer) hair cells of the chick's cochlea. *J. Neurosci.* **12**, 800–809 (1992).
5. Petersen, O. H. & Maruyama, Y. Calcium-activated potassium channels and their role in secretion. *Nature* **307**, 693–696 (1984).
6. Robitaille, R. & Charlton, M. P. Presynaptic calcium signals and transmitter release are modulated by calcium-activated potassium channels. *J. Neurosci.* **12**, 297–305 (1992).
7. Wu, Y. C., Ricci, A. J. & Fettiplace, R. Two components of transducer adaptation in auditory hair cells. *J. Neurophysiol.* **82**, 2171–2181 (1999).
8. Niu, X., Qian, X. & Magleby, K. L. Linker-gating ring complex as passive spring and Ca(2+)-dependent machine for a voltage- and Ca(2+)-activated potassium channel. *Neuron* **42**, 745–756 (2004).
9. Jiang, Y., Pico, A., Cadene, M., Chait, B. T. & MacKinnon, R. Structure of the RCK domain from the E. coli K+ channel and demonstration of its presence in the human BK channel. *Neuron* **29**, 593–601 (2001).
10. Quirk, J. C. & Reinhart, P. H. Identification of a novel tetramerization domain in large conductance K(ca) channels. *Neuron* **32**, 13–23 (2001).
11. Xia, X. M., Zeng, X. & Lingle, C. J. Multiple regulatory sites in large-conductance calcium-activated potassium channels. *Nature* **418**, 880–884 (2002).
12. Wu, Y., Yang, Y., Ye, S. & Jiang, Y. Structure of the gating ring from the human large-conductance Ca(2+)-gated K(+) channel. *Nature* **466**, 393–397 (2010).
13. Yuan, P., Leonetti, M. D., Pico, A. R., Hsiung, Y. & MacKinnon, R. Structure of the human BK channel Ca2+-activation apparatus at 3.0 A resolution. *Science* **329**, 182–186 (2010).
14. Ding, J. P., Li, Z. W. & Lingle, C. J. Inactivating BK channels in rat chromaffin cells may arise from heteromultimeric assembly of distinct inactivation-competent and noninactivating subunits. *Biophys. J.* **74**, 268–289 (1998).
15. Wang, Y. W., Ding, J. P., Xia, X. M. & Lingle, C. J. Consequences of the stoichiometry of Slo1 alpha and auxiliary beta subunits on functional properties of large-conductance Ca2+-activated K+ channels. *J. Neurosci.* **22**, 1550–1561 (2002).
16. Wallner, M., Meera, P. & Toro, L. Molecular basis of fast inactivation in voltage and Ca2+-activated K+ channels: a transmembrane beta-subunit homolog. *Proc. Natl. Acad. Sci. USA* **96**, 4137–4142 (1999).
17. Xia, X. M., Ding, J. P. & Lingle, C. J. Molecular basis for the inactivation of Ca2+- and voltage-dependent BK channels in adrenal chromaffin cells and rat insulinoma tumor cells. *J. Neurosci.* **19**, 5255–5264 (1999).
18. Xia, X. M., Ding, J. P. & Lingle, C. J. Inactivation of BK channels by the NH2 terminus of the beta2 auxiliary subunit: an essential role of a terminal peptide segment of three hydrophobic residues. *J. Gen. Physiol.* **121**, 125–148 (2003).
19. Chen, M. *et al.* Lysine-rich extracellular rings formed by hbeta2 subunits confer the outward rectification of BK channels. *PLoS One* **3**, e2114 (2008).
20. Zeng, X. H., Xia, X. M. & Lingle, C. J. Redox-sensitive extracellular gates formed by auxiliary beta subunits of calcium-activated potassium channels. *Nat. Struct. Biol.* **10**, 448–454 (2003).
21. Li, H. *et al.* Interaction sites between the Slo1 pore and the NH2 terminus of the beta2 subunit, probed with a three-residue sensor. *J. Biol. Chem.* **282**, 17720–17728 (2007).
22. Benzinger, G. R., Xia, X. M. & Lingle, C. J. Direct observation of a preinactivated, open state in BK channels with beta2 subunits. *J. Gen. Physiol.* **127**, 119–131 (2006).
23. Lingle, C. J., Zeng, X. H., Ding, J. P. & Xia, X. M. Inactivation of BK channels mediated by the NH(2) terminus of the beta3b auxiliary subunit involves a two-step mechanism: possible separation of binding and blockade. *J. Gen. Physiol.* **117**, 583–606 (2001).

24. Zhou, M., Morais-Cabral, J. H., Mann, S. & MacKinnon, R. Potassium channel receptor site for the inactivation gate and quaternary amine inhibitors. *Nature* **411**, 657–661 (2001).
25. Lee, U. S., Shi, J. & Cui, J. Modulation of BK channel gating by the ss2 subunit involves both membrane-spanning and cytoplasmic domains of Slo1. *J. Neurosci.* **30**, 16170–16179 (2010).
26. Long, S. B., Campbell, E. B. & Mackinnon, R. Crystal structure of a mammalian voltage-dependent Shaker family K+ channel. *Science* **309**, 897–903 (2005).
27. Zeng, X. H., Ding, J. P., Xia, X. M. & Lingle, C. J. Gating properties conferred on BK channels by the beta3b auxiliary subunit in the absence of its NH(2)- and COOH termini. *J. Gen. Physiol.* **117**, 607–628 (2001).
28. Carter, P. J., Winter, G., Wilkinson, A. J. & Fersht, A. R. The use of double mutants to detect structural changes in the active site of the tyrosyl-tRNA synthetase (Bacillus stearothermophilus). *Cell* **38**, 835–840 (1984).
29. Sadovsky, E. & Yifrach, O. Principles underlying energetic coupling along an allosteric communication trajectory of a voltage-activated K+ channel. *Proc. Natl. Acad. Sci. USA* **104**, 19813–19818 (2007).
30. Serrano, L., Horovitz, A., Avron, B., Bycroft, M. & Fersht, A. R. Estimating the contribution of engineered surface electrostatic interactions to protein stability by using double-mutant cycles. *Biochemistry* **29**, 9343–9352 (1990).
31. Yifrach, O. & MacKinnon, R. Energetics of pore opening in a voltage-gated K(+) channel. *Cell* **111**, 231–239 (2002).
32. Lv, C. *et al.* Four-turn alpha-helical segment prevents surface expression of the auxiliary hbeta2 subunit of BK-type channel. *J. Biol. Chem.* **283**, 2709–2715 (2008).
33. Zakharov, S. I. *et al.* Locations of the beta1 transmembrane helices in the BK potassium channel. *Proc. Natl. Acad. Sci. USA* **105**, 10727–10732 (2008).
34. Wu, R. S. *et al.* Location of the beta 4 transmembrane helices in the BK potassium channel. *J. Neurosci.* **29**, 8321–8328 (2009).
35. Wu, R. S. *et al.* Positions of β2 and β3 subunits in the large-conductance calcium- and voltage-activated BK potassium channel. *J. Gen. Physiol.* **141**, 105–117 (2012).
36. Orio, P. & Latorre, R. Differential effects of beta 1 and beta 2 subunits on BK channel activity. *J. Gen. Physiol.* **125**, 395–411 (2005).
37. Campbell, R. E. *et al.* A monomeric red fluorescent protein. *Proc. Natl. Acad. Sci. USA* **99**, 7877–7882 (2002).
38. Hess, B., Kutzner, C., Spoel, D. & Lindahl, E. GROMACS 4: Algorithms for highly efficient, load-balanced, and scalable molecular simulation. *J. Chem. Theory. Comput.* **4**, 435–447 (2008).

Acknowledgments

We thank Dr. Luyang Wang for valuable suggestions on this work. This work was supported by grants from the National Basic Research Program of China (2010CB529804), the National Science Foundation of China (30971179, 31170814, 31028006). The authors have no conflicts to disclose.

Author contributions

W. Z., C. L. and X. G. contributed to the biochemical assays. S. W. contributed to Homology Modeling. P. H., G. G., Z. Z., H. L., J. Y. and Y. W. performed electrophysiological experiments. P. H. and J. D. designed the experiments. W. Z. and P. H. analyzed the data. A. D. W. and J. D. wrote the paper. All authors reviewed the manuscript.

Additional information

Supplementary information accompanies this paper at http://www.nature.com/scientificreports

Competing financial interests: The authors declare no competing financial interests.

How to cite this article: Hou, P.P. *et al.* Inter-α/β subunits coupling mediating pre-inactivation and augmented activation of BK_{Ca}(β2). *Sci. Rep.* **3**, 1666; DOI:10.1038/srep01666 (2013).